Localization of Neuron Nucleuses in Microscopy Images with Convolutional Neural Networks

Arkadiusz Tomczyk[1], Bartłomiej Stasiak[1], Paweł Tarasiuk[1],
Anna Gorzkiewicz[2], Anna Walczewska[2] and Piotr S. Szczepaniak[1]
[1]*Institute of Information Technology, Lodz University of Technology, Wolczanska 215, 90-924 Lodz, Poland*
[2]*Department of Cell-to-Cell Communication, Medical University of Lodz,*

Keywords: Convolutional Neural Networks, Machine Learning, Fluorescent Microscope, Nucleus Localization.

Abstract: In this paper, an automatic method of neuron nucleuses localization in the images, taken with the fluorescent microscope, is presented. The proposed approach has two phases. During the first phase, a properly trained convolutional neural network acts as a non-linear filter which indicates regions of interest. The network architecture and specific method of its training are original concepts of the authors of this work. In the second phase, analysis of these regions allows to identify points representing positions of the nucleuses. To illustrate the method, images of neurons isolated from neonatal rat cerebral cortex were used. These images were inspected by a domain expert and all the visible nucleuses were manually annotated. This allowed not only to objectively assess the obtained detection results but it enabled the application of machine learning as well.

1 INTRODUCTION

Automatic analysis of images becomes a crucial task in a world where there are more and more image sources. To design proper algorithms, machine learning techniques can be used, where both models and parameters of these models can be selected automatically during the training phase. Application of machine learning requires, however, access to the domain knowledge, which usually is expressed in form of a train set which contains inputs and corresponding expected outputs. The gathering of this knowledge constitutes a separate, difficult task, which is even harder in the case of specialized images where the number of qualified domain experts is usually relatively small.

In this paper, neuron images, acquired with fluorescent microscope, are analyzed to localize all neuron nucleuses. For this purpose a two-stage approach is proposed, which in its first phase uses a convolutional neural network (CNN) (LeCun and Bengio, 1995) to find regions of interest. Since it is not a typical application of such networks, the proposed architecture can be considered as a main contribution of this paper. It should be emphasized that the conducted research was possible only thanks to the manually indicated nucleuses provided by a domain expert.

The paper is organized as follows: section 2 describes the similar works briefly, in section 3 the used data are characterized, in sections 4 and 5 the proposed approach and the obtained results are discussed, respectively and finally, the last section contains a short summary of the conducted research.

2 RELATED WORK

Application of convolutional neural networks to analyze microscopy images is a relatively new idea. In the literature some existing approaches can be found, which differ in: analyzed image type, the goal of image analysis, CNN application method, etc. All of them have, however, one common problem which needs to be overcome – availability of training data.

Localization and segmentation tasks are not areas of typical CNN applications. CNN is usually used as a part of a classifier which may assign labels to the whole image or to some of its regions when a moving window procedure is applied. For segmentation and localization tasks, this classic architecture is usu-

Tomczyk, A., Stasiak, B., Tarasiuk, P., Gorzkiewicz, A., Walczewska, A. and Szczepaniak, P.
Localization of Neuron Nucleuses in Microscopy Images with Convolutional Neural Networks.
DOI: 10.5220/0006753601880196
In *Proceedings of the 11th International Joint Conference on Biomedical Engineering Systems and Technologies (BIOSTEC 2018) - Volume 2: BIOIMAGING*, pages 188-196
ISBN: 978-989-758-278-3

ally modified, because at the output there should be an image of the same size as at the input. To achieve that goal, some up-scaling layers are added after some number of classic convolutional and pooling layers. Such approach was used in the works presented below:

- In (Sadanandan et al., 2017) the problem of cultured cell segmentation was considered. To overcome a problem with limited number of training samples, a method of automated train set generation was proposed. After normal image acquisition, cells were stained with fluorescent markers allowing to identify nucleuses and cytoplasmic regions. Then, images were used again, but this time simple segmentation techniques allowed to detect their positions and prepare the corresponding expected output masks for CNN training.

- In (Ho et al., 2017) 3D fluorescent microscopy images of rat kidney cells were segmented and the data was processed by a properly trained 3D CNN. In the case of 3D images, however, the difficulty of manual image annotation is even bigger than in 2D case, so to obtain sufficiently numerous train set, data augmentation procedures were used. These included modifications of image brightness and contrast as well as elastic deformations warping images locally.

- In (Quan et al., 2016), as a part of an approach similar to works mentioned above, the training data generation procedures were used (rotations, reflections, random noise) to increase the size of the train set. This time, however, 2D electron microscopy images were analyzed and the goal was cell membrane segmentation.

- In (Xie et al., 2016), the problem of cell counting was presented. In this work, CNN was trained to regress a cell spatial density distribution. To avoid problems with training data, both inputs and outputs were synthesized automatically. An interesting element of the method presented there is that two parallel regression networks were trained simultaneously and their results were combined to get the final response.

The solution presented in this work differs mainly in the type of the analyzed images and in the specific method of CNN application. Here, while the image processing is performed, the image size is not reduced. Consequently, all the feature maps have the same size and no up-scaling is required.

3 DATA

The images analyzed in this work contain neurons that were isolated from neonatal rat cerebral cortex. The cells were divided into four groups. The first is the control group where the cells were incubated in standard neuronal medium for 3 days. In three other groups, the standard neuronal medium was changed for the third day: the second group was incubated with medium collected from astrocytes culture, whereas the groups three and four were incubated with medium collected from the culture of astrocytes, that were earlier modified with two different polyunsaturated omega-3 fatty acids, DHA and EPA, respectively. After the time of incubation, the neurons were fixed and immunostained with primary monoclonal anti-β-Tubulin antibody and secondary antibody conjugated with fluorescent molecules. The fixed slides were analyzed and the pictures were taken using a fluorescent microscope.

The further aim of this research is to measure how the factors released to medium by the modified astrocytes influence neuronal wiring. The formation of neuronal projections and connections during development is crucial for the proper functioning of the nervous system. The recognition of neuronal nucleuses will help to determine localizations of the cell bodies on the picture, in order to further define the number, lengths and widths of the neuronal projections in proportion to the number of cells.

The set of available data contained 16 images which size is 1024×1024 pixels. An example image is shown in Fig. 1. In every image, the position of every neuron nucleus was manually indicated by a domain expert (Fig. 2), constituting a set of expected localization points $O^e = \{o_i^e : i = 1,\ldots,N^e\}$ where $o_i^e \in \{0,\ldots,1023\} \times \{0,\ldots,1023\}$. This set was further split into train, validation and test set which contained 8, 4 and 4 images, respectively. The initial analysis of the reference points revealed that the minimum pixel distance d between these points is equal to 8. This value will be used later in the presented experiments.

4 METHOD

The method of neuron nucleuses localization is composed of two, separately trained, phases. In the first phase, the specially designed fully convolutional neural network tries to approximately indicate image regions that are similar to nucleuses. It is a kind of a non-linear filter which should have a high response in the potentially interesting regions and low response

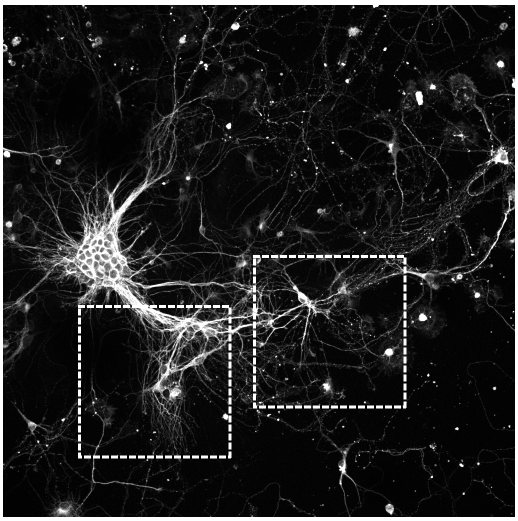

Figure 1: Representative fluorescence image of neurons stained with antibodies against beta-tubulin, class III conjugated with Alexa Fluor 488 acquired using a Zeiss microscope. The squares indicates the image regions, which, for better visibility, will be used further to illustrate the presented concepts (the original image size – 1024×1024 pixels, the region size – 300×300 pixels).

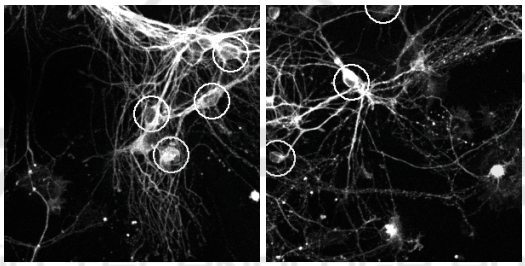

(a) (b)

Figure 2: Sample regions with manually indicated nucleuses. For better visibility the points given by an expert are surrounded with circles (circle radius – 20 pixels).

in the other places. In the second phase, the result of the filtration is analyzed to give a set of points that are suspected to be located within neuron nucleus area (one point per nucleus). Obviously, the found points do not need to precisely correspond with the reference points given by a domain expert. That is why a dedicated evaluation procedure is required to objectively measure the quality of the results. It can be used both to summarize the final results and to find the optimal parameters while training. All those elements are described in the further sections in details.

4.1 Convolutional Neural Network Architecture and Training

Convolutional neural networks are biologically inspired neural networks that succeeded in many tasks connected with image analysis (Cireşan et al., 2011; Krizhevsky et al., 2012). In typical applications, where they are used as image classifiers, they have a common general architecture in which after some number of convolutional layers, the resulting feature maps are processed by fully connected layers to give a final response (which is a form of predicted label encoding). The feature maps produced by the successive layers usually have decreasing sizes, which is caused both by the convolution itself (no additional padding is used) and by the pooling (e.g. max-pooling) layers.

In this work, the approach described above is not acceptable, since the CNN is supposed to work like a non-linear filter which, given an image, is able to produce the image of the same size after the filtration. That is why the architecture, firstly proposed in (Stasiak et al., 2017), will be used here instead. In this architecture fully connected layers are removed, in every convolutional layer the appropriate padding is added and no pooling layers are involved at all. The non-linearity of such a network is guaranteed by the non-linear activation functions (Fig. 3).

To train such a network, the output should be

given in a form of the expected, filtered image. In our case it must be prepared with usage of the reference points O^e given by an expert. The simplest solution could be generation of the whole black outputs, with only given points set to be white. After initial experiments it appeared, however, that this approach is not acceptable, as the network in the training process favors those combinations of weights that lead to the whole black output (the number of white pixels is very small in comparison with the size of the image and such a solution will constitute an attractive local minimum of a training loss function). The other solution could be to draw filled, white circles around the expected points with the radius big enough to avoid the problem mentioned above. This would, however, lead to another difficulty. Sufficiently big radius may cause that after the filtration, pairs of nucleuses that are very close to each other will be indistinguishable. That is why, further in this work, a different approach was proposed. The Gaussian function was used to describe the expected response around reference points. Such a response was generated in some area around every reference point and if some points were close to each other, the maximum response was selected (Fig. 4). The Gaussian function parameters were selected according to the visual field of the CNN (at the border of that field, Gaussian function value should decrease to 0.5). Such an expected output allows to train CNN using a classic Euclidean loss function L (regression problem).

The interesting property of the used architecture is the fact that it can be trained using smaller images (that refers to cutting, but not scaling) and after training it can be applied for full-size inputs (Stasiak et al., 2017). This property was also used in this work, where training images had size of 51×51 pixels (Fig. 4). Of course, to train the network properly. the set of these images had to be representative. That is why two groups of such images were generated. In the first group, there were images taken from the neighborhood of the reference points (positive samples). In the second group, 200 randomly located images were cut (negative samples) in such a way to not overlap with positive samples. Since the number of nucleuses is smaller than 200, this procedure gave unbalanced positive and negative sets. To avoid problems with training, the number of positive samples was increased by taking into account all the rotations of the positive images and by oversampling (the same image was repeated multiple times in the generated set). Positive and negative samples were generated from every full-size image and the corresponding expected output images in the train and validation sets were used to produce train (2312 positive and 1600 negative) and validation (1140 positive and 800 negative) sets of smaller images for network training.

In the further experiments, two architecture types were considered as presented in Fig. 3. The second model $M^+(K)$ differs from the first one $M^-(K)$ only with additional dropout layer (Srivastava et al., 2014) which was added before the final convolutional layer (K defines the number of kernels). Since the dropout probability is set to 50%, the number of filters in the last but one layer was doubled in $M^+(K)$. The proportion between the number of filters in successive layers and the size of the filters were selected based on the existing hints from the literature. In the initial layers filters are smaller, but their number is bigger. Both architectures have a visual field of size 23×23 pixels, which should be enough to cover single nucleus in the analyzed images.

4.2 Neuron Nucleuses Localization

The positions of the nucleuses cannot be extracted directly from the network output since, which is a consequence of the expected output type used for CNN training, the pixel values in filtered images change smoothly in the areas were nucleuses can be expected. To find them, a dedicated procedure was proposed where connected regions of pixels with intensity above the threshold t are searched for using region growing algorithm. The regions of area greater than a are rejected as overly general. The centers of gravity (expressed in image coordinates) of the regions found in this way constitute a preliminary set of the result points. The proper values of threshold t and area a can be selected automatically using full-sized training images.

To find a final set of points $O^r = \{o^r_j : j = 1,\ldots,N^r\}$ where $o^r_j \in \{0,\ldots,1023\} \times \{0,\ldots,1023\}$, additional post-processing needs to be performed, as the filtration output is not perfect. First, all the duplicates are removed. Next, if the distance between points is smaller than an expected minimum distance between nucleuses d, those points are merged together (their coordinates are averaged). To avoid a chain effect, this procedure is performed starting from points with the biggest number of such overly close neighbors. Merging is performed as long as there are points that could be merged.

4.3 Result Evaluation Procedure

To evaluate the results of nucleuses localization, two sets of points O^e and O^r must be compared. As it was already mentioned, since the nucleuses have some non-zero size, it cannot be expected that coor-

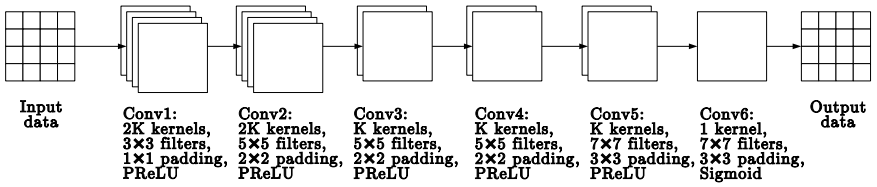

(a)

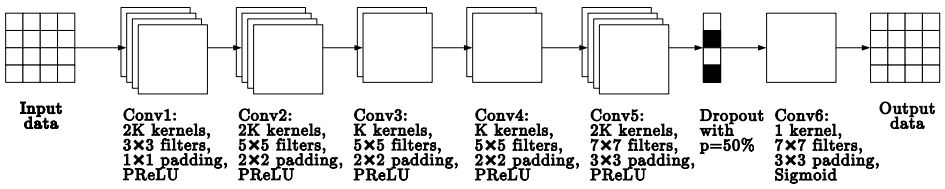

(b)

Figure 3: Architecture of the considered convolutional networks (K is equal to either 10 or 20): (a) - network without droput layer $M^-(K)$, (b) - network with dropout layer $M^+(K)$. All except the last convolutional layers use PReLU (parametrized rectified linear unit) and in the last layer sigmoid function is used to obtain values from $[0,1]$ interval. The last convolutional layer has only one kernel to generate one output image.

dinates of the expected and the found points will be the exactly the same. Consequently, some reasonable distance tolerance D should be assumed. If the distance between the expected point and the found point is smaller than this value, the corresponding nucleus can be considered to be found. Further the following notation will be used:

- $S_i^e = \{j = 1,\ldots,N^r : \rho(o_i^e, o_j^r) < D\}$ – a set of indexes of those result points that lie closer than D to the expected point o_i^e
- $S_j^r = \{i = 1,\ldots,N^e : \rho(o_j^r, o_i^e) < D\}$ – a set of indexes of those expected points that lie closer than D to the result point o_j^r

where ρ denotes the Euclidean metric.

Table 1: Selection of the best combination of parameters t and a for optimal network $M^+(20)$. Every cell contains averaged F_1 value calculated for 8 images in a train set. The highlighted cell indicates the optimal combination.

		a			
		100	**150**	**200**	**250**
t	**200**	0.492	0.570	0.593	0.592
	210	0.509	0.564	0.572	0.572
	220	0.522	0.556	0.555	0.555
	230	0.473	0.485	0.485	0.485
	240	0.382	0.381	0.381	0.381
	250	0.170	0.170	0.170	0.170

To compare the expected and the found points, two error types need to be considered. The first one checks *false positives*, i.e. the number of found points that do not correspond with any nucleus:

$$FP = \sum_{j=1}^{N^r} I(S_j^r = \emptyset). \tag{1}$$

The second one checks *false negatives*, i.e. the number of nucleuses that do not have corresponding detected point:

$$FN = \sum_{i=1}^{N^e} I(S_i^e = \emptyset). \tag{2}$$

In the notation presented in this paper, I is an indicator function which value is equal 1 if the given condition is true and 0 otherwise.

The above measures do not allow to fully evaluate the quality of the results, because those values need to be compared with the number of correctly identified nucleuses. Their number can be found, however, in two different ways as:

- a number of nucleuses that have at least one corresponding result point

$$TP^e = \sum_{i=1}^{N^e} I(S_i^e \neq \emptyset), \tag{3}$$

- a number of result points that have at least one corresponding nucleus

$$TP^r = \sum_{j=1}^{N^r} I(S_j^r \neq \emptyset). \tag{4}$$

Those numbers may differ if $|S_i^e| > 1$ or $|S_j^r| > 1$ (Fig. 5). Fortunately, this situation will not occur if $D = d/2$. Then $TP = TP^e = TP^r$ and the localization results can be evaluated using typical measures such as:

- *precision* – the percentage of correctly localized points

$$P = \frac{TP}{TP + FP}, \tag{5}$$

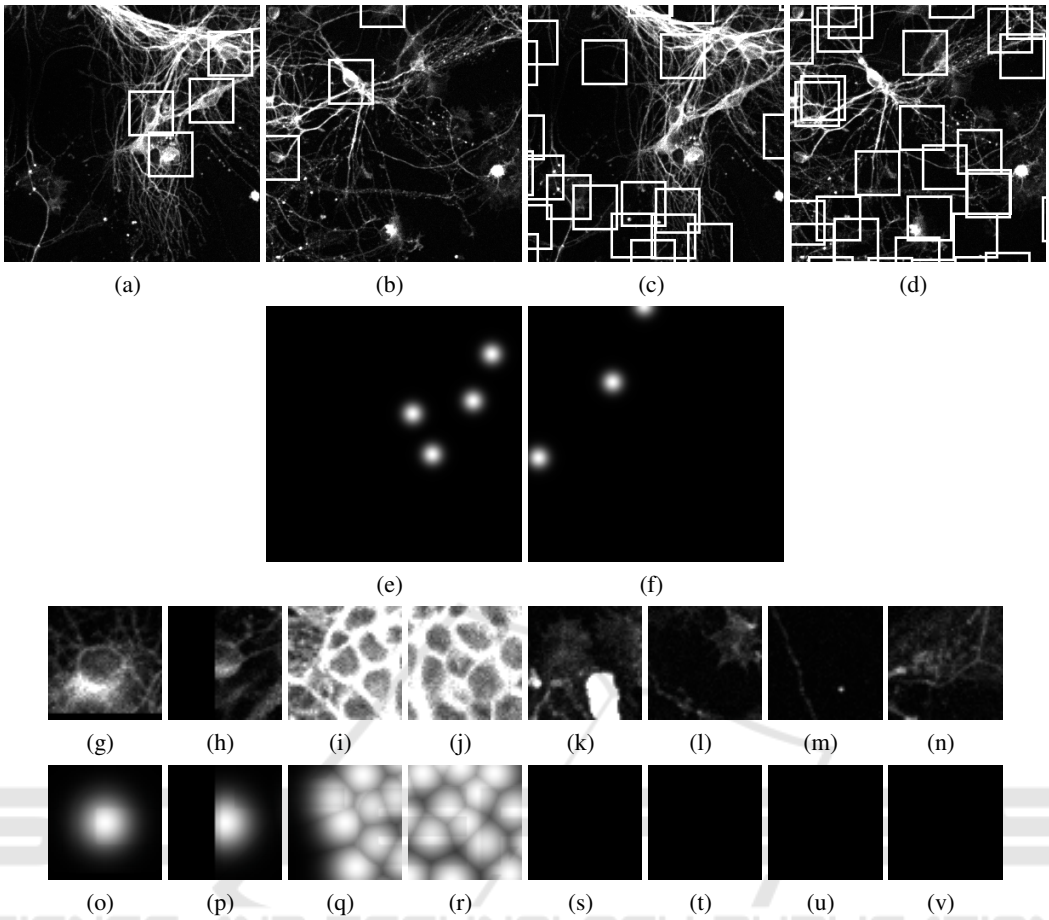

Figure 4: Convolutional training data (regions size – 51×51 pixels): (a), (b) - positions of positive samples generated around the reference points, (c), (d) - positions of positive samples selected randomly – they do not overlap with positive samples, (e), (f) - expected output with Gaussian functions generated around the reference points, (g) - (n) - examples of network inputs (4 positive samples and 4 negative samples), (o) - (v) - examples of the corresponding expected network outputs (4 positive samples and 4 negative samples).

Table 2: Comparison of the trained solutions. Average F_1 value on a validation set should allow to select solution with the greatest chance for generalization abilities. The highlighted row indicates the optimal solution.

solution	final L		avarage F_1		
	train	**validation**	**train**	**validation**	**test**
$M^-(10), t = 220, a = 150$	17.89	20.10	0.49	0.35	0.51
$M^+(10), t = 210, a = 200$	18.75	20.02	0.51	0.39	0.51
$M^-(20), t = 220, a = 200$	13.07	12.49	0.55	0.42	0.50
$M^+(20), t = 200, a = 200$	12.91	12.79	0.59	0.44	0.45

- *recall* – the percentage of the correctly localized nucleuses

$$R = \frac{TP}{TP+FN}. \tag{6}$$

For a perfect solution, both these values should be close to 1. To obtain a single value, they are usually combined using harmonic mean:

$$F_1 = \frac{2PR}{P+R}. \tag{7}$$

Such a single averaged value will be further used to select a proper solution and to find proper values of the parameters t and a.

5 RESULTS

The results presented in this work required CNN training and usage of the trained CNN. It would not be

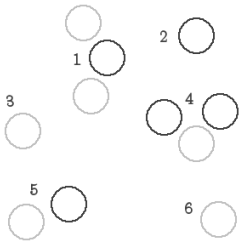

Figure 5: For evaluation purposes, the reference points (dark gray) needed to be compared with the found points (light gray) – the distances between points are bigger than in real cases for better visibility. The following situations are possible: 3, 6 – detections unrelated to the expected points, 2 – missing detection, 5 – good detection, 1 – one point detected twice, 4 – merged points. Detections are considered with some distance tolerance.

possible to perform with an acceptable performance if a proper hardware with GPU units were not available. For the experiments described further, NVIDIA Tesla P100 card and Caffe faramework (Jia et al., 2014) were used.

Table 3: Results of application of optimal network $M^+(20)$ for all available images. In the second and third column the numbers of the expected nucleuses and numbers of localized nucleuses are presented, respectively. The highlighted row indicates a case which was used in figures presented in this work.

image	$\lvert O^e \rvert$	$\lvert O^r \rvert$	P	R	F_1
train set					
1	20	20	0.50	0.50	0.50
2	10	12	0.75	0.90	0.82
3	51	45	0.58	0.51	0.54
4	29	23	0.43	0.34	0.38
5	28	26	0.58	0.54	0.56
6	26	27	0.67	0.69	0.68
7	33	35	0.74	0.79	0.76
8	92	116	0.45	0.57	0.50
validation set					
9	41	34	0.44	0.37	0.40
10	11	13	0.62	0.73	0.67
11	15	16	0.19	0.20	0.19
12	28	24	0.54	0.46	0.50
test set					
13	33	33	0.61	0.61	0.61
15	37	34	0.29	0.27	0.28
16	43	47	0.47	0.51	0.49
17	33	29	0.45	0.39	0.42

5.1 Experiments

In the presented experiments, two variants ($K = 10$ and $K = 20$) of both convolutional neural network architectures (without and with the dropout layer) were considered. Consequently, 4 neural networks were trained using 3912 images of size 51×51. In the beginning, the learning rate was equal to 0.00001 and was decreased every 100 iterations with factor 0.995. The momentum was equal to 0.95 and maximum number of iterations was set to 100000. For these parameters, the training process took from 2 to 5 hours depending on the network architecture. In Fig. 6, an example of changes of Eculidean loss can be observed both on the train set and on the validation set (1940 images of size 51×51). The similar characteristic of the training process was observed for all 4 networks. Since the validation error did not increase, no evident overfitting problem was noticed and the final network obtained from the training was used for the further computations. In Fig. 8, sample filtration results of the trained network are presented.

The next step was selection of the parameters t and a required in the second phase of the proposed approach. For that purpose, selected combinations of these parameters were tested for all 4 networks. Every combination was evaluated using the train set with 8 images of size 1024×1024. To sum up the evaluation procedure with a single numerical value, the average F_1 value was calculated. Results are presented in Tab. 1. It allowed to select optimal parameter combination for every network which can be found in Tab. 2.

When the network is trained and above parameters are found, the solutions are ready for nucleus localization. There are, however, 4 solutions, and one must be selected as the final one. In order to do that, solutions were evaluated using average F_1 on the validation set with 4 images of size 1024×1024. Again, the obtained values can be found in Tab. 2. This procedure allowed to select as a final solution – the network $M^+(20)$. Sample results generated by this solution are depicted in Fig. 7. The summary of the results for all 16 available images is presented in Tab. 3.

5.2 Analysis

Analyzing results presented in Tab. 2, the first conclusion is that networks with bigger number of kernels K allowed to get a better averaged F_1 measure both for the training and the validation set. This observation is quite intuitive, since more complex network should have bigger flexibility, allowing it to learn to perform more complex filtering. There is no significant difference of final Euclidean loss L values between the architectures with and without dropout. It could be expected, however, that for dropout-enabled networks, the overfitting problem will not be observed too early and, in consequence, for these architectures the dif-

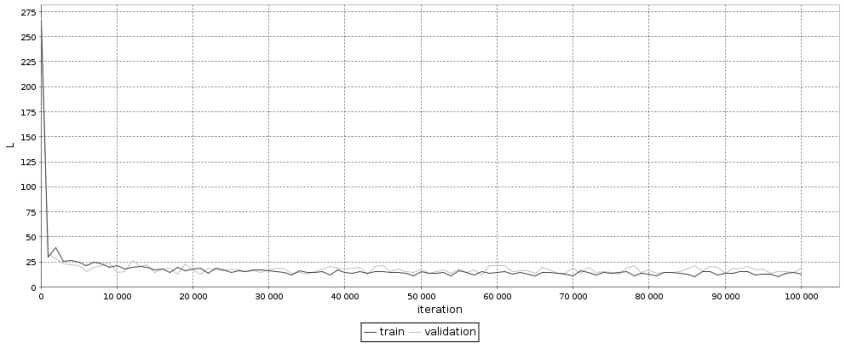

Figure 6: The value of loss function L during the training process of optimal network $M^{+}(20)$. This value is calculated both on train set (dark gray) and validation set (light gray). No evident overfitting problem can be observed.

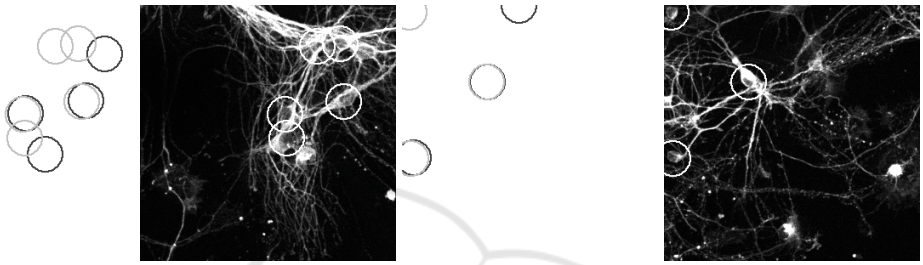

(a) (b) (c) (d)

Figure 7: Sample localization results for optimal network $M^{+}(20)$ after its training and selection of corresponding t and a parameters: (a), (c) - comparison of expected points (dark gray) and detected points (light gray), (b), (d) - the predicted localization of nucleuses within the original image.

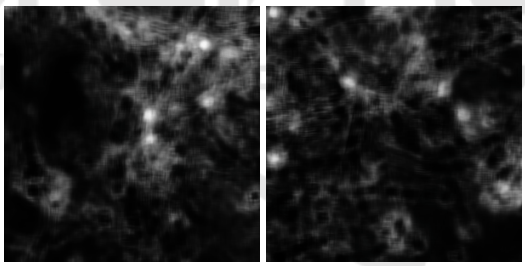

(a) (b)

Figure 8: Sample outputs of the optimal neural network $M^{+}(20)$ after its training (result of filtration). Higher response can be observed in the regions where nucleuses are expected.

ference between train and validation errors should be a smaller than int the case of architectures without dropout. But since, as it was already mentioned, an overfitting was not observed at all in Fig. 6, this expected trend is not visible in the presented results.

Interesting are, however, the averaged F_1 values obtained for the test set (presented in Tab. 2), where a tendency is quite opposite to the trend observed for the train set and the validation set. The only explanation of such an observation is a small number of the available images. As it was decribed in Sec. 3, the images come from 4 different groups. In the presented work, the possible differences between those groups were not taken into account and, as it was checked after the experiments, the pseudo-random assignment of images to the train, validation and test sets caused that one group was overrepresented in the test set.

Further analysis of the obtained results depicted in Fig. 8 and Fig. 7 reveals what are the other problems of the proposed solution:

- Nucleuses and their surrounding areas can have a very different characteristics.
- There are structures in the images similar to the nucleuses, that should not be detected (region on the left of the top nucleus in Fig. 7b).
- There are very dark (almost invisible) nucleuses (nucleus at the top of Fig. 7d).

Most of these problems could be overcome, as it is often with machine learning based techniques, if more samples of the training data were available. Additionally, some image pre-processing could be helpful here to increase local contrast in dark areas. Nevertheless, the obtained preliminary results are undoubtedly encouraging.

6 SUMMARY

In this work, we present a method of automatic localization of the neuron nucleuses in the images acquired with fluorescent microscope. This method is based on the convolutional neural network which is trained to act as a non-linear filter. These filtration results are analyzed further to indicate possible localizations of nucleuses. An original element of the presented work is the way a CNN concept was used for the filtration task. Also the result evaluation technique can be considered as an interesting idea for similar works. This approach allowed not only to objectively measure the quality of the proposed solution, but to find the optimal parameters used in the second phase of the described approach as well.

The obtained results leave a lot of space for further improvement. Some of the possible ideas were already mentioned in the previous section. To improve the filtration results, maybe the number of positive and negative samples could be increased. There is no problem with the second group, but for obvious reasons the number of positive samples is limited. The main attempt to overcome this problem was taking into account all 4 rotations of these samples. This, however, may not cover the whole variety of visible structures, since CNN is not invariant to input rotation. To solve this problem, CNN modification described in (Tarasiuk and Pryczek, 2016) may be of use. Data augmentation methods, such as brightness and contrast modifications or local elastic deformations, can be of use here as well. Also a bigger visual field could allow the filter to take more information about the pixel surrounding into account. All those aspects are under further investigation.

ACKNOWLEDGEMENTS

This project has been partly funded with support from National Science Centre, Republic of Poland, decision number DEC-2012/05/D/ST6/03091.

REFERENCES

Cireşan, D. C., Meier, U., Masci, J., Gambardella, L. M., and Schmidhuber, J. (2011). Flexible, high performance convolutional neural networks for image classification. In *Proceedings of the Twenty-Second International Joint Conference on Artificial Intelligence - Volume Volume Two*, IJCAI'11, pages 1237–1242. AAAI Press.

Ho, D. J., Ch., F., Salama, P., Dunn, K. W., and Delp, E. J. (2017). Nuclei Segmentation of Fluorescence Microscopy Images Using Three Dimensional Convolutional Neural Networks. In *IEEE Conference on Computer Vision and Pattern Recognition Workshops (CVPRW) 2017*, pages 834–842.

Jia, Y., Shelhamer, E., Donahue, J., Karayev, S., Long, J., Girshick, R., Guadarrama, S., and Darrell, T. (2014). Caffe: Convolutional Architecture for Fast Feature Embedding. *arXiv preprint arXiv:1408.5093*.

Krizhevsky, A., Sutskever, I., and Hinton, G. E. (2012). Imagenet classification with deep convolutional neural networks. In Pereira, F., Burges, C. J. C., Bottou, L., and Weinberger, K. Q., editors, *Advances in Neural Information Processing Systems 25*, pages 1097–1105. Curran Associates, Inc.

LeCun, Y. and Bengio, Y. (1995). Convolutional networks for images, speech, and time-series. In Arbib, M. A., editor, *The Handbook of Brain Theory and Neural Networks*. MIT Press.

Quan, T. M., Hildebrand, D. G. C., and Jeong, W. (2016). FusionNet: A deep fully residual convolutional neural network for image segmentation in connectomics. *CoRR*, abs/1612.05360.

Sadanandan, S. K., Ranefall, P., Le Guyader, S., and Whlby, C. (2017). Automated Training of Deep Convolutional Neural Networks for Cell Segmentation. *Scientific Reports*, 7(1).

Srivastava, N., Hinton, G., Krizhevsky, A., Sutskever, I., and Salakhutdinov, R. (2014). Dropout: A Simple Way to Prevent Neural Networks from Overfitting. *J. Mach. Learn. Res.*, 15(1):1929–1958.

Stasiak, B., Tarasiuk, P., Michalska, I., Tomczyk, A., and Szczepaniak, P. (2017). Localization of Demyelinating Plaques in MRI using Convolutional Neural Networks. In *Proceedings of the 10th International Joint Conference on Biomedical Engineering Systems and Technologies (BIOSTEC 2017) - Volume 2: BIOIMAGING*, pages 55–64. SCITEPRESS.

Tarasiuk, P. and Pryczek, M. (2016). Geometric Transformations Embedded into Convolutional Neural Networks. *Journal of Applied Computer Science*, 24(3):33–48.

Xie, W., Noble, J., and Zisserman, A. (2016). Microscopy cell counting and detection with fully convolutional regression networks. *Computer Methods in Biomechanics and Biomedical Engineering: Imaging & Visualization*, pages 1–10.